Determining the Chemical Reactivity Trends of Pd/Ru(0001) Pseudomorphic Overlayers: Core-Level Shift Measurements and DFT Calculations

E. Golfetto,[†,‡] A. Baraldi,[*,†,§] M. Pozzo,[‖] D. Alfè,[‖,⊥] A. Sala,[†,#] P. Lacovig,[†,∇] E. Vesselli,[†,§] S. Lizzit,[∇] G. Comelli,[†,§] and R. Rosei[†,‡,§]

Physics Department and Center of Excellence for Nanostructured Materials, University of Trieste, Via Valerio 2, I-34127 Trieste, Italy, Laboratorio "Nanotecnologie per l'Energia", Consorzio per la Fisica, S.S. 14 Km 163.5, 34149 Trieste, Italy, Laboratorio TASC INFM-CNR, AREA Science Park, S.S. 14 Km 163.5, 34012 Trieste, Italy, Department of Earth Sciences and Thomas Young Centre@UCL, University College London, Gower Street, London WC1E 6BT, United Kingdom, Department of Physics and Astronomy, University College London, Gower Street, London WC1E6BT, United Kingdom, London Centre for Nanotechnology, University College London, Gower Street, London WC1E6BT, United Kingdom, and Sincrotrone Trieste S.C.p.A., S.S. 14 Km 163.5, I-34149 Trieste, Italy

Received: September 4, 2009; Revised Manuscript Received: October 12, 2009

We have addressed the problem of determining a reliable *experimental descriptor* of surface chemical reactivity by measuring Pd and Ru $3d_{5/2}$ core-level shifts of the Pd_n/Ru(0001) pseudomorphic overlayer system ($n = 0-3$) by high resolution X-ray photoelectron spectroscopy. We find a linear relationship between the calculated theoretical changes of the d-band center position projected on each Ru and Pd atomic layer (which is, according to the Hammer and Norskov d-band model, a good *theoretical descriptor* of chemical reactivity) and the corresponding core-level shifts, both for the Ru atomic planes and for the Pd overlayers. Core-level shifts, therefore, should be considered as reliable *experimental descriptors* of chemical reactivity in the same sense (and with similar limitations) of the *theoretical descriptor* d-band center. Final-state effect contributions to the shifts do not obscure this trend.

1. Introduction

Catalytic processes pervade worldwide industrial production, to the point that it is difficult to overstate their role in modern economies,[1] and their importance, therefore, justifies the intense ongoing research efforts in this field. The daunting problems posed by a "sustainable growth" are pressing toward more stringent requirements for less expensive and more efficient catalysts.[2] The advances in surface science techniques, first-principles calculations, and synthesis methods are providing new insight into the atomic/molecular level surface chemistry governing heterogeneous catalytic activity and offer the groundwork for a true rational design conceptual frame for developing novel catalysts.[3−5] To this end, however, it is still necessary to develop new techniques, which may afford the direct determination of chemical reactivity. This is particularly true for metal alloys, which often exhibit a superior catalytic performance compared with the single constituents and are, for this reason, widely used in industrial processes.[6] Understanding the manipulation of a catalyst's properties by alloying, therefore, has been of increasing significant importance in catalyst research.[7,8]

On alloying a basic metal with a second element, different effects arise, which deeply affect the catalyst's behavior. Indeed, it is well-known that ligand, stress/strain, and ensemble effects depend on the nature and the amount of the second elemental component alloyed into the base metal, as well as on the ensuing structural and geometrical changes. As a consequence, tracing the origin of observed catalytic reactivity modifications on each individual effect is a very difficult task.

In this context, bimetallic pseudomorphic overlayer (PO) systems are of special interest since, by preparing a suitable structure with a specific composition, they offer the possibility of tailoring surface chemical reactivity in controlled and reproducible ways.[8,9] POs represent model systems simple enough for developing a systematic understanding of the relationship between microscopic structure and catalytic activity; at the same time, they offer the opportunity of preparing a broad variety of overlayer/substrate structures and compositions, still with the option of increasing the degree of complexity in a sizable way.

POs' chemical reactivity is still governed, however, by a subtle interplay of electronic and geometrical effects,[10,11] whose relative importance has been proven difficult to disentangle.[12] A fairly simple theoretical framework for understanding chemical reactivity properties of transition metals (TM) and TM alloys (the so-called "d-band model"), has been developed using the density functional theory (DFT).[13] The model has been very successful in explaining chemical trends in the interaction of atoms and molecules with TMs and has clarified the role of substrate composition,[14] structure,[15] and of local atom coordination.[16] The metal surface reactivity is found to be directly related to the d-band center energy position (ε_d), calculated with respect to the Fermi energy E_F. Indeed, it has been found that a clear

---

[*] To whom correspondence should be addressed. E-mail: baraldi@elettra.trieste.it. Phone: +39-0403758719. Fax: +39-0403758776.

[†] University of Trieste.

[‡] Consorzio per la Fisica.

[§] Laboratorio TASC INFM-CNR, AREA Science Park.

[‖] Department of Earth Sciences and Thomas Young Centre@UCL, University College London.

[⊥] Department of Physics and Astronomy, and London Centre for Nanotechnology, University College London.

[#] Present address: Fritz-Haber-Institut der Max-Planck-Gesellschaft, Faradayweg 4-6, D-14195 Berlin-Dahlem, Germany.

[∇] Sincrotrone Trieste S.C.p.A.

10.1021/jp908568v

linear relationship between ε_d and the adsorption energy of most common atoms and molecules holds.[17−19] Although DFT calculations of the surface-projected d-band center are reasonably easy to accomplish (even for rather complex geometries, such as, e.g., stepped surfaces), the task of determining experimentally (using ultraviolet photoelectron spectroscopy) the surface d-band density of states (DOS) of POs and disentangling it from the bulk DOS component is extremely difficult because of band dispersion and overlapping contributions from species in different chemical and geometrical environment.

An interesting alternative approach was employed by using X-ray photoelectron spectroscopy (XPS). It has been long known that electron core-level (CL) binding energies (BE) provide an accurate local probe of the electronic structure changes of an atom in different environments. In their pioneering investigation on supported monolayers on different metal substrates, Rodriguez and Goodman[20] reported a correlation between the changes in the desorption temperature of adsorbates and the relative substrate CL shifts, indicating that core-level measurements can be a powerful tool for examining surface chemical reactivity. However, the interpretation of CL shifts of the surface metal atoms based on charge-transfer reasoning was questioned by DFT calculations[21,22] indicating that, although CL shifts can give important information on surface reactivity changes, final state contributions can be significant, in particular, for noble metals, such as Cu and Ag, where the low density of states at the Fermi level yields a rather inefficient screening of the core hole. Nevertheless, for a large number of TM systems (both clean and adsorbate-covered), high resolution X-ray photoemission spectroscopy (HRPES) experiments at modern synchrotron radiation facilities[23] have shown a linear relationship between surface core-level shifts (SCLS) changes and the theoretically determined ε_d shifts, thus indicating that, in these cases, the screening correction magnitude is rather small compared with the overall trend of initial-state shifts.[24−29] Because of these properties, the idea of using the changes of SCLS as an experimental descriptor of the trends in surface chemical reactivity has been put forward.[30]

In the following, we present the results of HRPES experiments, paralleled by DFT calculations, with the aim of investigating the electronic structure of pseudomorphically grown Pd layers on Ru(0001) and of determining the correlation between their reactivity properties and observed SCLS changes. The Pd/Ru system has a number of interesting properties that make it particularly suitable for our purpose. It has been shown long ago that Pd overlayers grow pseudomorphically on Ru(0001) surfaces.[31] Pd has a large negative segregation energy with respect to Ru,[32] which prevents intermixing up to very high temperatures and allows, therefore, moderate annealing procedures. Moreover, the system has already been characterized by a variety of techniques, both experimentally[33−38] and theoretically[39,40] (mostly, however, at the Pd single-monolayer level).

In this paper, we show that CL shifts for Ru and Pd species are directly proportional to the calculated d-band center shifts, thus demonstrating that, for this alloy, the magnitude of the screening correction does not obscure the overall trends in the initial state shifts. Therefore, also for this PO system, CL shifts contain relevant electronic structure information and can be considered a reliable descriptor of surface chemical reactivity trends.

2. Experimental Setup, Sample Preparation, And Data Analysis

The characterization of the Pd growth process was done in a ultra-high-vacuum (UHV) chamber equipped with an ion gun, a four degrees of freedom manipulator with heating and cooling capabilities, and a physical vapor deposition Pd evaporator. The Ru crystal was cleaned by cycles of Ar^+ sputtering (10 $\mu A \cdot cm^{-2}$), annealing to 1570 K, and O_2 treatment at 5×10^{-7} mbar in the temperature range of 1000−1200 K, for removing the residual carbon. A final annealing to 1500 K was done to induce oxygen desorption. After this procedure, the sample showed a sharp (1 × 1) low-energy electron diffraction (LEED) pattern with low background and flat terraces about 500 Å wide, as results from the profile analysis of the LEED spots.

The Pd evaporator consists of a 0.25 mm diameter high-purity Pd wire, which can be resistively heated. The evaporation filament is housed in a tantalum cylinder, with an opening of about 20 mm diameter at the front face for depositing the metal directly onto the Ru substrate, while preventing Pd evaporation onto UHV system components. The metal source was gradually heated and then held at the evaporation temperature for a fixed amount of time. The pressure in the UHV systems was always kept below 4×10^{-10} mbar for preventing the adsorption of background impurities on the bimetallic surface. To characterize the growth process, high k-resolution electron diffraction data were taken using an Omicron Spot Profile Analysis LEED. By means of this instrument (transfer width of ∼1000 Å) high-quality reciprocal space maps and zero-order diffraction beam spot profiles were acquired at fixed energies. Reproducible deposition of impurity-free metal overlayers was routinely achieved. The LEED beam profiles at different Pd coverage were acquired at room temperature. The characterization of the Pd growth mode and the coverage determination were performed in out-of-phase Bragg condition of the zero-order diffraction beam, which corresponds to an electron energy of 85 eV. The specular diffraction spot intensity modulation and its line profile changes were measured for monitoring the thermodynamic growth mechanism.[41] The periodic modulation of the diffraction intensity and the absence of extra-tails at the zero-order diffraction spot sides are indicative of a Frank−van der Merwe heteroepitaxial growth, while the appearance of extra peaks between maxima is linked to the formation of Pd islands with a characteristic correlation length. Pd deposition at $T = 320$ K with a flux of about 0.9 ML/minute (followed by subsequent annealing at 670 K) resulted in a layer-by-layer growth up to 2 MLs, as already reported in previous investigations.[31] During formation of the third layer, a slight disorder takes place with the fourth layer starting to form before the completion of the third one. Once the best evaporation conditions (filament current, evaporation time, substrate temperature, and post deposition annealing temperature) for a layer-by-layer growth of Pd on Ru(0001) were determined, the evaporator was moved to the SuperESCA beamline for the HRPES measurements.[42]

The SuperESCA experimental station is composed of a preparation chamber for cleaning and growth and a main chamber for the photoemission measurements. The latter hosts a Phoibos electron energy analyzer (mean radius = 150 mm) with a delay-line detector, a VG manipulator with 5 degrees of freedom with heating and liquid nitrogen cooling capabilities, and a VG rear-view LEED optics. The base pressure during measurements was 1×10^{-10} mbar. The Pd and Ru $3d_{5/2}$ photoemission measurements were performed at normal photoelectron emission conditions with the sample at room temperature and a photon energy of 410 eV. The overall energy

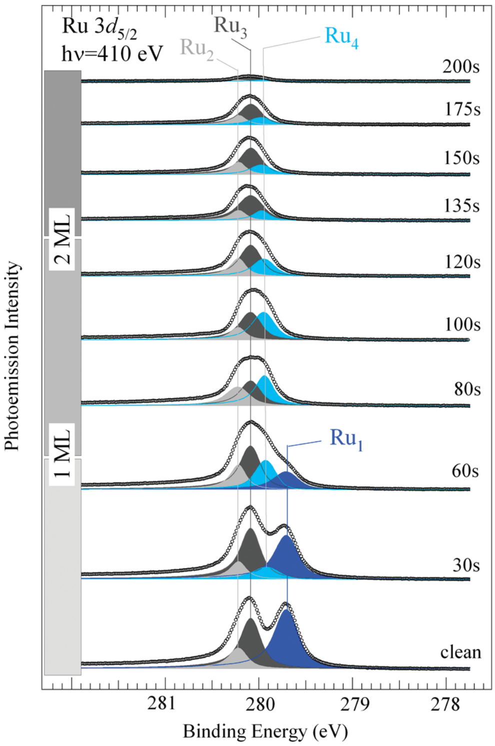

Figure 1. Series of high-energy resolution Ru $3d_{5/2}$ core-level spectra collected at $T = 300$ K after different Pd deposition times. The solid lines superimposed to the experimental data (open circles) are the result of the final fits; the colored curves correspond to the different Ru components. The individual components are plotted after linear background removal.

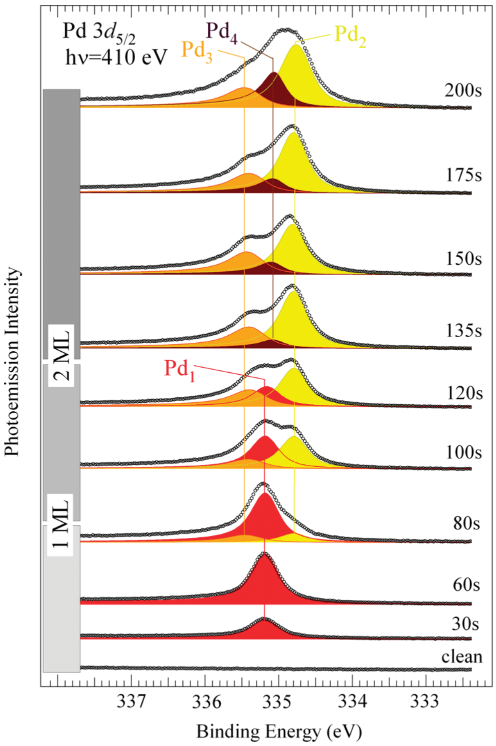

Figure 2. Series of high-energy resolution Pd $3d_{5/2}$ core-level spectra collected at $T = 300$ K after different Pd deposition times. The solid lines superimposed to the experimental data (open circles) are the result of the final fits; the colored curves correspond to the different Ru components. The individual components are plotted after linear background removal.

resolution (electron energy analyzer and X-ray monochromator) was 40 meV for both Pd and Ru $3d_{5/2}$ core-level spectra. The electron binding energies are referred to the Fermi energy position, measured under the same experimental conditions (photon energy, analyzer setup, and surface temperature). HRPES measurements in the C 1s, S 2p, and O 1s core-level regions confirmed the absence of contaminants.

All the photoemission data have been fitted by a convolution of a Doniach−Sunjic (DS) function and a Gaussian, which accounts for the phonon broadening and the contribution of the instrumental resolution. A linear background was also subtracted. The DS profile contains a Lorentzian distribution (described by the Γ parameter) arising from the finite core hole lifetime and an asymmetry parameter α to account for electron−hole pairs' excitation at the Fermi level.

3. Experimental Results

Figures 1 and 2 show series of Ru $3d_{5/2}$ and Pd $3d_{5/2}$ CL spectra, respectively, for different Pd deposition times, up to completion of three Pd MLs. As previously reported,[43,44] the Ru $3d_{5/2}$ CL spectrum of the clean surface (before starting Pd deposition) consists of three components highlighted in Figure 1: a peak centered at 279.70 ± 0.02 eV, originating from Ru atoms of the first layer (Ru_1, dark blue); a peak at 280.21 ± 0.02 eV due to second-layer atoms (Ru_2, light gray), and finally, a third component at 280.08 ± 0.02 eV due to deeper, bulk layers (Ru_3, dark gray). The best-fit parameter values are180 ± 20 meV for the Lorentzian width, 0.08 ± 0.02 meV for the asymmetry parameter, and 120 ± 20 meV for the Gaussian width of the bulk component, while the first- and the second-layer Gaussian widths were 170 and 90 meV, respectively, in good agreement with the values found in previous determinations. All the fits gave very small and structureless residuals, proving the accuracy of the method.

Upon submonolayer Pd deposition, (exposure times of 30 and 60 s), a single component grows in the Pd $3d_{5/2}$ spectral region, at a BE of 335.15 ± 0.02 eV (Pd_1, red curve, Figure 2). In the corresponding Ru $3d_{5/2}$ spectra, the Ru_1 component intensity drops markedly, and a new peak (Ru_4, light blue, Figure 1) with a SCLS shift of −180 meV appears. The progressive growth of this component in the 30 and 60 s spectra is paralleled by a decrease of the Ru_1 peak intensity (−40% and −75%, respectively). This is expected because the fraction of Ru "clean" surface atoms (i.e., not coordinated to adsorbed Pd atoms) decreases progressively as the Pd coverage increases. At the same time, the signal originating from Ru bulk and Ru second-layer atoms is progressively attenuated by the growing Pd overlayer.

At 80 and 120 s Pd deposition times (corresponding, as determined by our SPA-LEED measurements, to intermediate coverages between 1 and 2 ML), the Ru_1 signal vanishes, while the corresponding Pd $3d_{5/2}$ spectrum undergoes large modifications. A tail at higher BE and a shoulder at lower BE with respect the Pd_1 component appear, and the fit requires now two extra components only, shifted by +220 ± 40 meV (Pd_3, orange curve, Figure 2) and −370 ± 40 meV (Pd_2, yellow curve, Figure 2), with respect to the Pd_1 component, respectively. For a Pd deposition time of 135 s (corresponding to a ∼2 ML coverage), the Pd_1 population has disappeared, and the Pd $3d_{5/2}$ spectrum can be decomposed by using only the Pd_2 and Pd_3 peaks. Two components, shifted by 530 meV, in the Pd $3d_{5/2}$ spectrum above 1 ML Pd coverage were already reported by Andersen et al.;[38] the presence of a third component was most probably hidden by the lower experimental resolution of their measurements.

TABLE 1: Calculated *d*-Band Center Energy Positions ε_d (with Respect to the Fermi Energy E_F) for the Clean Ru(0001) and Pd(111) Surfaces and for Three Pseudomorphic Pd Overlayers on Ru(0001)

E_d (eV)	Ru(0001)	Pd(111)	1 Pd ML Ru(0001)	2 Pd MLs Ru(0001)	3 Pd MLs Ru(0001)
Pd-I					−1.71
Pd-II				−1.76	−2.07
Pd-III		−1.63	−2.12	−2.40	−2.39
Ru-I	−1.42		−1.69	−1.76	−1.74
Ru-II	−1.88		−1.86	−1.86	−1.85
Ru-III	−1.79		−1.79	−1.79	−1.80

At deposition times exceeding 135 s, the spectrum undergoes further modifications: the spectral minimum slowly starts to be filled by a new component (Pd_4, brown curve, Figure 2) at a BE of 335.04 ± 0.02 eV. Although its BE is very similar, this new peak has a different physical origin than Pd_1. As it will be shown in the following, it arises from second-layer atoms in a 3 ML Pd film. The lowest BE component seems to be moderately sensitive to this further Pd thickness increase: on increasing the coverage from 2 to 3 Pd MLs, it appears to shift only by about 40 meV toward lower BE. At these Pd coverages, all the Ru $3d_{5/2}$ spectral components are still present in the spectra, but with progressively decreasing intensity.

4. Theoretical Methods and Results

DFT calculations have been performed using the generalized gradient approximation (GGA) of Perdew, Burke, and Ernzerhof known as PBE.[45] The ionic cores have been described using ultrasoft pseudopotentials (USPP)[46] and single particle orbitals expanded in plane waves with a planewave cutoff of 30 Ry and a cutoff for the charge density of 240 Ry. The code used for the calculations was PWscf.[47] Surfaces have been modeled using a slab geometry, with up to eight atomic layers and a vacuum region of 12 Å. Two atomic layers have been fixed to the bulk interatomic distance, while the topmost remaining atomic layers have been allowed to relax. Convergence with respect to the thickness of the vacuum region has been carefully tested. Integration inside the Brillouin zone has been performed by summation over 12 × 12 × 1 Monkhorst−Pack grids of special points. A smearing function of Methfessel−Paxton[48] (product of a Gaussian times a first-order Hermite polynomial) and width = 0.13 eV has been used throughout.

The position of the d-band center E_d with respect to the Fermi energy E_F has been calculated as

$$E_d = \int_{-\infty}^{E_0} dE(E - E_F)pd(E)$$

where $pd(E)$ is the projection of the electronic density of states onto atomic orbitals of type d and E_0 is the cutoff energy that we chose to be 5 eV above the Fermi energy. Our theoretical results for the Ru and Pd clean metals, and for three different pseudomorphic overlayer systems (1, 2, and 3 Pd MLs on Ru(0001)), are summarized in Table 1.

5. Discussion

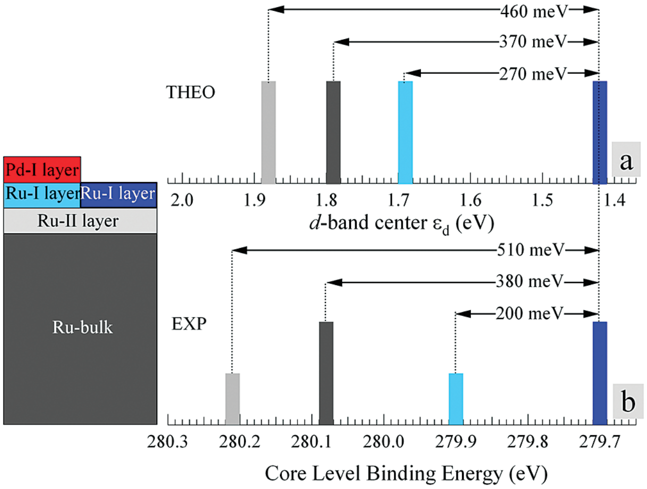

Figure 3. Comparison of experimental binding energy of Ru $3d_{5/2}$ core-level components and theoretical layer-projected d-band centers. (a) Shifts of the Ru d-band center with respect to the clean Ru surface. (b) Shifts of the Ru $3d_{5/2}$ core-level binding energies with respect to the clean Ru surface layer core level. The inset on the left shows schematically the physical system for which the comparison is done.

Figure 3 shows a comparison of the Ru $3d_{5/2}$ core-level shifts measured after 30 s of Pd evaporation time with the calculated d-band center shifts ε_d. Panel a shows schematically the ε_d values (calculated with respect to the clean Ru surface ε_d value), while panel b shows the corresponding CL BEs. By choosing the first layer (surface) BE as the origin of the shifts, the second layer's CL shift is 460 meV, while the third layer atoms' (representative of bulk atoms) shift is 370 meV.

As already mentioned, the Ru spectrum presents an extra component with respect to the clean surface situation (light blue in Figure 3b, at a shift of 200 meV), originating from the Ru surface atoms on which Pd atoms have adsorbed (see inset). The corresponding projected d-band center shift is 270 meV. The overall correspondence is satisfactory and confirms that the contribution of screening (always below 100 meV for the clean Ru(0001) surface[43]) does not obscure the initial-state trend. Final-state corrections, however, would be needed for obtaining an accurate quantitative agreement with the measured data.

In the following, we discuss in detail the Pd spectra because their behavior is more closely connected to the chemical significance of our results.

As already described in section 3, after 30 s of Pd deposition (corresponding to about 0.4 Pd ML), a single isolated peak appears at 335.15 eV BE. This feature linearly grows with the Pd deposition time. The $3d_{5/2}$ Pd CL for a clean Pd(111) surface has been previously measured at a BE of 334.60 eV,[49] so we conclude that the adsorption process of Pd adatoms on a Ru(0001) surface causes a Pd $3d_{5/2}$ BE change of 550 meV. Because the atom coordination number for both surfaces (Ru(0001) and Pd(111)) is the same (i.e., 9), the shift of 550 meV originates mainly from a combination of ligand and stress effects. Indeed, the Ru−Ru interatomic distance is known to be slightly smaller (−1.8%) than the Pd−Pd distance.

Our DFT calculations for a clean Pd surface layer (of Pd metal) and for a Pd PO on Ru(0001) give ε_d values of 1.63 and 2.12 eV, respectively. These values are schematically compared with Pd $3d_{5/2}$ BE changes in Figure 4a,b.

According to the d-band model of chemical reactivity, such large energy downshift ($\Delta\varepsilon_d \sim -30\%$) should correspond to a dramatic reduction of adsorbate binding energies. Indeed, Behm and co-workers[39] find a 30% reduction of deuterium adsorption energy on a Pd ML deposited on Ru(0001), with respect to the adsorption energy on a Pd(111) surface. Moreover, Pallassana et al. reported a significant larger binding strength of ethylene on Pd(111) (−62 kJ/mol) when compared with a Pd monolayer on Ru(0001) (−31 kJ/mol).[50]

Panel d in Figure 4 shows the position of the Pd $3d_{5/2}$ spectral components after a 120 s Pd deposition time (corresponding to

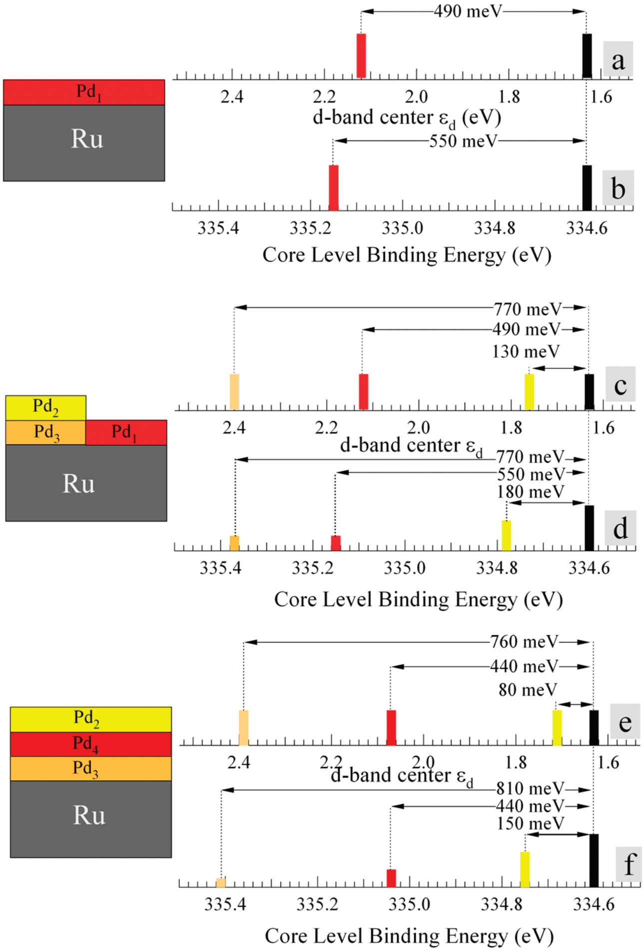

Figure 4. Comparison of experimental binding energy of Pd $3d_{5/2}$ core-level components and theoretical layer-projected d-band centers for Pd_n ($0 < n \leq 3$) overlayers deposited on Ru(0001): shift of the Pd d-band center and $3d_{5/2}$ CL for (a, b) 1 Pd pseudomorphic overlayer, (c, d) Pd_n layers with $1 < n \leq 2$, and (e, f) Pd_n layers with $n = 3$. The insets on the left show schematically the physical systems for which the comparisons are done. Both CL and d-band center shifts are referred to the clean Pd(111) surface CL and d-band center.

1.8 Pd MLs). In principle, after completion of 2 Pd MLs, two peaks should be present in our spectra (originating from the outermost surface layer and from the interface layer with the Ru substrate). The surface CL components of our HRPES data reflect this situation: two major peaks are found at 770 and 180 meV with respect to the pure Pd surface peak. In addition, the spectrum at this coverage shows a third (weak) component, at a 550 meV energy shift. This component is at the same energy as the Pd peak in Figure 4a, and we, therefore, interpret it as originating from Pd atoms adsorbed on Ru and not yet covered by the second Pd layer (which is still incomplete). According to our DFT calculations, the energy center of the d-band is found at 2.40 eV, while the surface-atoms-projected ε_d lies at 1.76 eV. The shifts of ε_d with respect to a pure Pd surface layer are, therefore, 770 and 130 meV, respectively (see panel c in Figure 4). According to the d-band model, this means that the surface chemical reactivity has now substantially increased with respect to the situation of a single Pd ML adsorbed on Ru, but it is lower than in the case of a pure Pd surface.

Finally, panels e and f in Figure 4 depict the situation after 200 s of Pd deposition, when nearly 3 MLs of Pd have been deposited. At 3 MLs of Pd coverage on Ru, we expect three peaks to appear in the Pd $3d_{5/2}$ spectrum (one for each layer), and this is, indeed, what happens. Also, the theoretical DFT results give three different E_d values, at 80, 440, and 760 meV with respect to the ε_d of the Pd clean surface first layer.

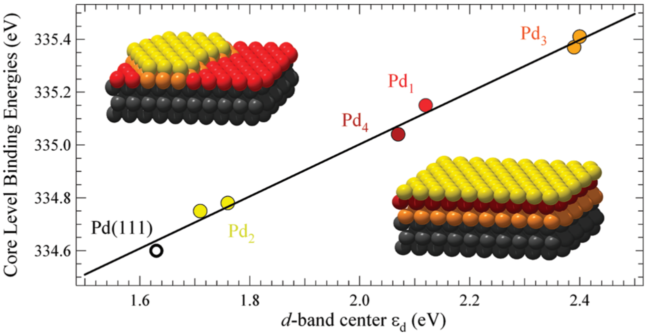

Figure 5. Relationship between Pd $3d_{5/2}$ core-level components, arising from Pd overlayers and corresponding DFT calculated d-band centers. The circles in the figure are color-coded according to the insets in the upper left and lower right of the figure. The relationship is strikingly linear, showing that final-state effects do not obscure the core-level shift trends, as indicators of chemical reactivity.

In summary, the CL shift of the topmost Pd layer results to be 550 meV when only 1 ML is present, 180 meV when 2 MLs have been deposited, and finally, 150 meV when there are 3 Pd MLs. The very small difference of the shifts between the 2 and 3 ML situation shows that the ligand effect originating from the Ru interface basically does not contribute significantly beyond the third Pd atomic layer. The remaining shift, therefore, can originate only from the strain caused by the Pd layer maintaining the Ru lattice parameter. We conclude that the CL BE analysis allows a proper distinction between ligand- and strain-effect contributions. In the case of the Pd/Ru(0001), we find that the ligand-effect contribution is twice as large as the stress-effect. A compendium of our experimental and theoretical results for 1, 2, and 3 Pd MLs is shown in Figure 5.

It can be immediately perceived that a very clear linear relationship (linear correlation coefficient = 0.99 ± 0.01) between the measured surface core-level binding energies and the calculated d-band centers holds. We argue, therefore, that, although measured CL BEs are definitely affected by final-state contributions, intrinsic to the photoemission process, still their contribution does not obscure the overall trends for Pd overlayers on the Ru(0001) system. Our results confirm that, also, for the POs, SCLS changes are a useful experimental descriptor of the projected d-band center of transition metals and, therefore, according to the d-band model, of TMs' chemical reactivity.

Acknowledgment. We acknowledge financial support from Sincrotrone Trieste S.C.p.A., from Regione Friuli Venezia Giulia through the project "Catalizzatori nanostrutturati per la produzione di idrogeno e sperimentazione su prototipi di fuel-processor", and from Fondazione CRTrieste through Consorzio per la Fisica, Trieste. A.B. warmly acknowledges Prof. Franco Jona from Stony Brook University for the donation of the "Old Lady" UHV chamber where the LEED experiments have been performed. A.B. acknowledges precious technical support from Angst-Pfister.

References and Notes

(1) Hagen, J. Economic Importance of Catalysts. *Industrial Catalysis*, 2nd ed.; Wiley-VCH Verlag GmbH & Co. KGaA: Weinheim, Germany, 2006; pp 425−428.

(2) Schlögl, R. *Angew. Chem., Int. Ed.* **1998**, *37*, 2333.

(3) Besenbacher, F.; Chorkendorff, I.; Clausen, B. S.; Hammer, B.; Molenbroek, A. M.; Nørskov, J. K.; Stensgaard, I. *Science* **1998**, *279*, 1913.

(4) Greeley, J.; Mavrikakis, M. *Nat. Mater.* **2004**, *3*, 810.

(5) Greeley, J.; Jaramillo, T. F.; Bonde, J.; Chorkendorff, I. B.; Nørskov, J. K. *Nat. Mater.* **2006**, *5*, 909.

(6) Sinfelt, J. H. *Bimetallic Catalysts: Discoveries, Concepts, and Applications*; Wiley: New York, 1983.

(7) Rodriguez, J. A.; Goodman, D. W. *Science* **1992**, *257*, 897.

(8) Gross, A. *Top. Catal.* **2006**, *37*, 29.

(9) Alayoglu, S.; Nilekar, A. U.; Mavrikakis, M.; Eichhorn, B. *Nat. Mater.* **2008**, *7*, 333.

(10) Hammer, B.; Nørskov, J. K. *Adv. Catal.* **2000**, *45*, 71.

(11) Schlapka, A.; Lischka, M.; Gross, A.; Käsberger, U.; Jakob, P. *Phys. Rev. Lett.* **2003**, *91*, 016101.

(12) Kitchin, J. R.; Nørskov, J. K.; Barteau, M. A.; Chen, J. G. *Phys. Rev. Lett.* **2004**, *93*, 156801.

(13) Mavrikakis, M.; Hammer, B.; Nørskov, J. K. *Phys. Rev. Lett.* **1998**, *81*, 2819.

(14) Hammer, B. *Top. Catal.* **2006**, *37*, 3.

(15) Hammer, B.; Nørskov, J. K. *Surf. Sci.* **1995**, *343*, 211.

(16) Hammer, B.; Nørskov, J. K. *Nature* **1995**, *376*, 238.

(17) Hammer, B.; Nielsen, O. H.; Nørskov, J. K. *Catal. Lett.* **1997**, *46*, 31.

(18) Pallassana, V.; Neurock, M.; Hansen, L. B.; Hammer, B.; Nørskov, J. K. *Phys. Rev. B* **1999**, *60*, 6146.

(19) Abild-Pedersen, F.; Greeley, J.; Studt, F.; Rossmeisl, J.; Munter, T. R.; Moses, P. G.; Skulason, E.; Bligaard, T.; Nørskov, J. K. *Phys. Rev. Lett.* **2007**, *99*, 016105.

(20) Rodriguez, J. A.; Goodman, D. W. *Science* **1992**, *257*, 897.

(21) Hennig, D.; Ganduglia-Pirovano, M. V.; Scheffler, M. *Phys. Rev. B* **1996**, *53*, 10344.

(22) Ganduglia-Pirovano, M. V.; Kudrnovsky, J.; Scheffler, M. *Phys. Rev. Lett.* **1997**, *78*, 1807.

(23) The high surface sensitivity, which can be obtained at the third generation synchrotron radiation beamlines, originates from a number of experimental unique capabilities, such as the ability of selecting the photon energy in such a way that photoemitted electrons have the minimum escape depth kinetic energy, and using grazing angle emission. The possibility of distinguishing shifts as small as 20 meV rests, however, on the possibility of choosing core levels of relatively small intrinsic line width, such as the Ru and Pd $3d_{5/2}$ levels in the present work.

(24) Bianchettin, L.; Baraldi, A.; de Gironcoli, S.; Lizzit, S.; Petaccia, L.; Vesselli, E.; Comelli, G.; Rosei, R. *Phys. Rev. B* **2006**, *74*, 45430.

(25) Bianchettin, L.; Baraldi, A.; Vesselli, E.; de Gironcoli, S.; Lizzit, S.; Petaccia, L.; Comelli, G.; Rosei, R. *J. Phys. Chem. C* **2007**, *111*, 4003.

(26) Bianchettin, L.; Baraldi, A.; de Gironcoli, S.; Vesselli, E.; Lizzit, S.; Petaccia, L.; Comelli, G. Rosei. *J. Chem. Phys.* **2008**, *128*, 114706.

(27) Baraldi, A.; Bianchettin, L.; Vesselli, E.; de Gironcoli, S.; Lizzit, S.; Petaccia, L.; Zampieri, G.; Comelli, G.; Rosei, R. *New J. Phys.* **2007**, *9*, 143.

(28) Baraldi, A. *J. Phys.: Condens. Matter* **2008**, *20*, 93001.

(29) Bianchettin, L.; Baraldi, A.; de Gironcoli, S.; Vesselli, E.; Lizzit, S.; Comelli, G.; Rosei, R. *J. Phys. Chem. C* **2009**, *113*, 13192.

(30) Baraldi, A.; Lizzit, S.; Comelli, G.; Kiskinova, M.; Honkala, K.; Nørskov, J. K. *Phys. Rev. Lett.* **2004**, *93*, 046101.

(31) Park, C. *Surf. Sci.* **1988**, *203*, 395.

(32) Ruban, A. V.; Skriver, H. L.; Nørskov, J. K. *Phys. Rev. B* **1999**, *59*, 15990.

(33) Rodriguez, J. A.; Campbell, R. A.; Goodman, D. W. *J. Vac. Sci. Technol., A* **1991**, *9*, 1698.

(34) Campbell, R. A.; Rodriguez, J. A.; Goodman, D. W. *Phys. Rev. B* **1992**, *46*, 7077.

(35) Hartmann, H.; Diemant, T.; Bergbreiter, A.; Bansmann, J.; Hoster, H. E.; Behm, R. J. *Surf. Sci.* **2009**, *603*, 1439.

(36) Hartmann, H.; Diemant, T.; Bansmann, J.; Behm, R. J. *Surf. Sci.* **2009**, *603*, 1456.

(37) Andersen, T. H.; Li, Z.; Hoffmann, S. V.; Bech, L.; Onsgaard, J. *J. Phys.: Condens. Matter* **2002**, *14*, 7853.

(38) Andersen, T. H.; Bech, L.; Li, Z.; Hoffmann, S. V.; Onsgaard, J. *Surf. Sci.* **2004**, *559*, 111.

(39) Rodriguez, J. A. *Surf. Sci.* **1994**, *303*, 366.

(40) Wu, R.; Freeman, A. J. *Phys. Rev. B* **1995**, *52*, 12419.

(41) Horn-von Hoegen, M. *Z. Kristallogr.* **1999**, *214*, 591.

(42) Baraldi, A.; Comelli, G.; Lizzit, S.; Kiskinova, M.; Paolucci, G. *Surf. Sci. Rep.* **2003**, *49*, 169.

(43) Lizzit, S.; Baraldi, A.; Groso, A.; Reuter, K.; Ganduglia-Pirovano, M. V.; Stampfl, C.; Scheffler, M.; Stichler, M.; Keller, C.; Wurth, W.; Menzel, D. *Phys. Rev. B* **2001**, *63*, 205419.

(44) Lizzit, S.; Zhang, Y.; Kostov, K. L.; Petaccia, L.; Baraldi, A.; Larciprete, R.; Menzel, D.; Reuter, K. *J. Phys.: Condens. Matter* **2009**, *21*, 134009.

(45) Perdew, J. P.; Burke, K.; Ernzerhof, M. *Phys. Rev. Lett.* **1996**, *77*, 3865.

(46) Vanderbilt, D. *Phys. Rev. B* **1990**, *41*, 7892.

(47) Baroni, S.; Dal Corso, A.; de Gironcoli, S.; Giannozzi, P. http://www.pwscf.org; see also http://www.quantum-espresso.org.

(48) Methfessel, M.; Paxton, A. *Phys. Rev. B* **1989**, *40*, 3616.

(49) Surnev, S.; Sock, M.; Ramsey, M. G.; Netzer, F. P.; Wiklund, M.; Borg, A.; Andersen, J. N. *Surf. Sci.* **2000**, *470*, 171.

(50) Pallassana, V.; Neurock, M. *J. Catal.* **2000**, *191*, 301.

JP908568V